Irradiance Variations of a Pyranometer due to Leveling Issues

Joshua Peterson[1], Adagia Latta[1]

[1]University of Oregon, Eugene OR, USA

***Abstract* — Pyranometers, widely used for measuring global horizontal irradiance (GHI), rely on precise leveling to ensure reliable data. Leveling issues, whether caused by improper installation, environmental factors, or mechanical degradation, can introduce errors in irradiance measurements. This study investigates the impact of pyranometer leveling deviations on calibration responsivity. First, the relationship between bubble level position and tilt angle was established by purposefully adjusting sensor levels and recording the corresponding bubble displacements. Then, sensors were calibrated in the horizontal configuration, and a geometric model was developed to predict how the responsivity would change if the sensor were tilted by a known amount (approximately 0.07°, corresponding to the bubble halfway to the edge of the level vial). The predicted tilt effect was compared against the natural day-to-day measurement variability observed during the horizontal calibration. Results show that for tilts at the bubble-in-circle level, the geometric calibration bias is smaller than the day-to-day measurement noise, confirming that standard bubble-level alignment is sufficient for component summation calibrations.**

Index Terms — solar irradiance, pyranometer, global horizontal irradiance, GHI, sensor level, sensor tilt, calibration, responsivity

I. Introduction

Solar energy research depends on precise solar irradiance measurements, with pyranometers playing a critical role in applications such as photovoltaic (PV) performance monitoring, solar forecasting, and system degradation studies. Accurate leveling of pyranometers is essential, as even small misalignments can introduce systematic errors that compromise data quality and long-term reliability.

One example where sensor level is particularly critical is the outdoor calibration of pyranometers using the component sum method [1, 2, 3]. In this approach, the responsivity (R) of a pyranometer is calculated according to (1).

$$R = \frac{\mu V}{DNI * cos(Z) + DHI} \qquad (1)$$

Where R is the responsivity of the device under test (DUT) in μV/(W/m²), μV is the output signal of the DUT, DNI is the reference direct normal irradiance (W/m²), DHI is the reference diffuse horizontal irradiance (W/m²), and Z is the solar zenith angle.

If the DUT in (1) is slightly tilted from horizontal, the pyranometer receives a different irradiance than a properly leveled reference sensor. This misalignment results in variations in calculated responsivity that can distort calibration results. Such variations are difficult to isolate from other influencing factors, including directional response and temperature dependence.

Pyranometers are typically leveled using bubble (spirit) levels; however, their high sensitivity makes precise alignment challenging in practice. Even with meticulous setup, bubbles frequently remain slightly off-center due to effects such as thermal expansion or mechanical shifting of the support structure. Unlike previous studies [4, 5, 6] that relied on long-term datasets, this work develops a geometric model to predict the calibration bias from small tilts and compares the predicted effect against measured day-to-day variability. The focus is to determine whether tilts at the bubble-in-circle level meaningfully affect calibration results.

II. Bubble Level Measurement Experimental Setup

Nine pyranometers were mounted on a large, rigid plate equipped with adjustable set bolts. The sensors included three Kipp & Zonen CMP11s, three Hukseflux SR20s, and three Eppley PSPs. Each sensor was installed on an independent leveling platform, allowing accurate individual leveling prior to plate adjustment. Fig. 1 shows a photograph of the experimental setup. The set bolts were spaced 406 mm apart in an equilateral triangle pattern, giving a triangle height of 352 mm. The bolts were 12.7 mm (½-inch) in diameter with a thread spacing of 1.95 mm. With this configuration, a 1/8 turn of a set bolt produced an angular change of approximately 0.034°. The tilt angle for any adjustment is given by (2), where N is the number of turns.

$$\theta = \arctan\left(N \times \frac{1.95\ \text{mm}}{352\ \text{mm}}\right) \qquad (2)$$

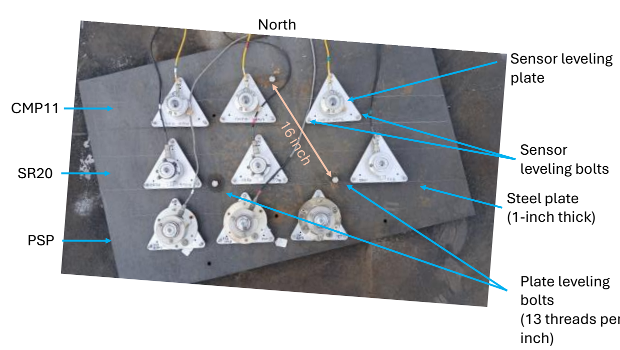

Fig 1. Experimental setup showing nine pyranometers mounted on the leveling platform with three adjustable set bolts. North is toward the top of the image.

The bolt adjustment was performed in successive increments of ±1/8, ±1/4, ±3/8, ±1/2, and ±1 turn. Between positive and negative rotations, the bolt was returned to the zero position and the bubble was confirmed to come back to the center position. At each increment, the bubbles were allowed to settle, and a photograph was taken of each sensor with the bolt position recorded.

To quantify bubble displacement from the photographs, three distances were measured in each image. These are the diameter of the bubble level (D), the diameter of the bubble itself (d), and the distance from the nearest edge of the level to the bubble edge (L). Fig. 2 gives a schematic diagram of the situation. From these measurements, a normalized displacement metric was defined according to (3), where R = D/2 and r = d/2. This ratio is independent of photograph zoom and provides a consistent measure of bubble displacement.

$$c' = \frac{R - r - L}{R - r} \quad (3)$$

When the bubble is perfectly centered, L + r = R and c' = 0. When the bubble edge touches the outer edge of the level vial, L = 0 and c' = 1. For the CMP11 and SR20, the painted reference circle sits approximately halfway to the vial edge. In practice, an operator judges leveling by the position of the bubble relative to this painted circle. The amount of air in the bubble varies from sensor to sensor, but in general the bubble is smaller than the reference circle. Estimating the bubble to be halfway out of the painted circle (center of bubble on the circle line) corresponds to c' of approximately 0.5.

Fig. 3 shows a scatter plot of c' versus θ for all nine sensors, with linear fits for each sensor type. The CMP11 and SR20 sensors have very similar trend lines, while the older PSP has a significantly less sensitive bubble.

Using the linear fits from Fig. 3, the tilt angle corresponding to specific bubble positions can be determined. For the CMP11 and SR20, the bubble halfway out of the painted circle (c' = 0.5) corresponds to a tilt of approximately 0.07°, and the bubble at the edge of the circle (c' = 1.0) corresponds to approximately 0.13°. The PSP, with its less sensitive level, requires much larger tilts to produce the same bubble displacement. These values are summarized in Table 1.

The 0.07° tilt represents a realistic scenario where an operator has leveled the sensor but the bubble remains slightly off-center, roughly halfway outside the painted circle. This is a common condition in field installations and calibration setups where perfect centering is difficult to achieve over extended periods of time. This value is used as the representative situation for the geometric modeling that follows. A second, larger tilt of 0.5° is also modeled to illustrate what would happen if the bubble were well outside the circle.

Table 1. Tilt angle corresponding to bubble level position for each sensor type.

Sensor	Sensor tilt (°) Bubble halfway out (c'=0.5)	Sensor tilt (°) Bubble at edge (c'=1.0)
CMP11	0.07°	0.13°
SR20	0.07°	0.13°
PSP	0.45°	0.89°

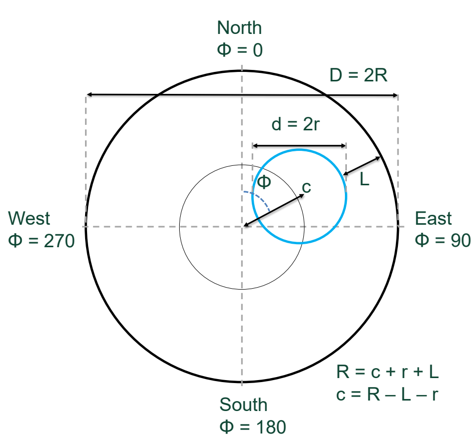

Fig 2. Schematic diagram of the bubble level measurement geometry showing the level diameter (D), bubble diameter (d), and edge distance (L) used to compute the normalized displacement c'.

III. Calibration Data Collection

Calibration data were collected at the University of Oregon Solar Radiation Monitoring Laboratory (44.05°N, 123.09°W). Reference instruments included an Eppley Absolute Cavity Radiometer for DNI and a Kipp & Zonen CMP22 for DHI. All data were sampled at 2-second intervals. Three days of horizontal calibration data were collected in May and June 2025 under clear-sky conditions.

Data were filtered to retain only stable periods: DNI between 200 to 1100 W/m², DHI between 40 to 150 W/m², rolling standard deviation of DNI below 2 W/m² over 60-second windows, and solar zenith angle below 80°. The goal of this filtering is to remove periods of variable sky conditions where the irradiance values are rapidly changing.

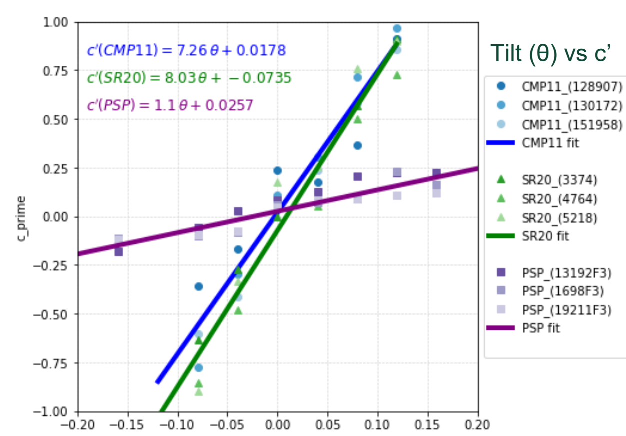

Fig 3. Normalized bubble displacement (c') versus tilt angle (θ) for all nine sensors with linear fits for each sensor type (CMP11, SR20, PSP).

The responsivity of each sensor was computed for each 2-second sample using (1) and is presented in Fig. 4. The day-to-day variation in responsivity is the dominant feature in the data. Although the sensors were maintained horizontal throughout, changes in atmospheric conditions (water vapor, pressure, temperature) cause the responsivity to vary from one day to the next. It was originally suspected that small leveling errors might be responsible for this variation, motivating this study. The goal is to determine whether sensor tilt can explain the observed variations in responsivity, or whether something else is the primary driver. In the modeling analysis that follows, a tilt angle of 0.07° is used. This corresponds to the bubble halfway out of the painted circle, as established in Section II.

To quantify the effect of tilt on calibration, a geometric model is developed starting from measured quantities. The DUT horizontal sensor output (μV_{horiz}) is measured directly. The reference irradiance (GHI_{ref}) is measured from independent reference instruments according to (4), where DNI is the direct normal irradiance, DHI is the diffuse horizontal irradiance, and Z is the solar zenith angle. The horizontal responsivity is computed from these two measured quantities using (5).

$$\mathrm{GHI_{ref}} = \mathrm{DNI} \cdot \cos(\mathrm{Z}) + \mathrm{DHI} \tag{4}$$

$$\mathrm{R_{horiz}} = \frac{\mu \mathrm{V_{horiz}}}{\mathrm{GHI_{ref}}} \tag{5}$$

Now consider a sensor that is tilted slightly, but the experimenter is unaware of the issue. For small tilt angles, the diffuse component on the tilted surface is approximately equal to the horizontal diffuse because the sky view factor remains essentially unchanged. Only the direct beam projection is affected. The irradiance on the tilted surface is given by (6), where the angle of incidence is computed according to (7). In (7), θ is the sensor tilt magnitude, A is the solar azimuth angle, and φ is the direction the tilted surface faces (0° for north, 90° for east, 180° for south, 270° for west).

$$\mathrm{POA} = \mathrm{DNI} \cdot \cos(\mathrm{AOI}) + \mathrm{DHI} \tag{6}$$

$$\mathrm{Cos(AOI)} = \cos(\mathrm{Z}) \cdot \cos(\theta) + \sin(\mathrm{Z}) \cdot \sin(\theta) \cdot \cos(\mathrm{A} - \varphi) \tag{7}$$

The tilted sensor produces a voltage proportional to the POA irradiance it receives, using the sensor's true responsivity as the conversion factor (8). We assume that R_{horiz} represents the true responsivity of the sensor. In other words, if a sensor with responsivity R_{horiz} were positioned at a tilt of θ, it would receive POA irradiance and generate a corresponding output voltage μV_{tilted}.

$$\mu \mathrm{V_{tilted}} = \mathrm{R_{horiz}} \times \mathrm{POA} \tag{8}$$

From this proxy μV_{tilted}, a tilted responsivity can be computed. During calibration, the experimenter is unaware of the tilt and divides by the horizontal reference GHI_{ref}, not by POA. This gives the responsivity that would have been reported for the tilted sensor according to (9). Put another way, the sensor outputs a voltage based on what it actually receives (POA), but the calibration assumes it received GHI_{ref}. This mismatch is the source of the tilt error.

$$R_{tilt} = \frac{\mu \mathrm{V_{tilted}}}{GHI_{ref}} \tag{9}$$

With both R_{horiz} and R_{tilt} defined, the percent difference between them is given by (10). Substituting (4) through (9) into (10) and simplifying, the DHI terms cancel, leaving only the direct beam projection (11).

$$\%\mathrm{diff} = \frac{(\mathrm{R_{tilt}} - \mathrm{R_{horiz}})}{\mathrm{R_{horiz}}} * 100 \tag{10}$$

$$\%\mathrm{diff} = \frac{\mathrm{DNI}}{\mathrm{GHI_{ref}}} * \left(\cos(\mathrm{AOI}) - \cos(\mathrm{Z})\right) * 100 \tag{11}$$

In (11), the percent error is the product of two factors. The ratio DNI/GHI_{ref} represents the fraction of total irradiance that comes from the direct beam; only this fraction is sensitive to tilt. The term (cos(AOI) - cos(Z)) represents the geometric change in beam projection due to the tilt; it depends on the tilt angle, the solar zenith angle, and the alignment between the tilt direction and the sun azimuth. When either factor is small (overcast skies or sun directly overhead), the tilt error vanishes. For a 0.07° tilt at solar noon in Eugene (Z = 21°, DNI = 900 W/m^2, GHI = 940 W/m^2), (11) evaluates to approximately 0.04%.

Fig. 4 presents the main result of this study in a 3x3 grid (three sensors by three columns). The left column shows the measured responsivity versus solar azimuth for three horizontal calibration days. The center and right columns show the percent difference from the median responsivity at each azimuth bin, where the median is computed across all three days for each 5° azimuth bin. In all three columns, the gray band represents the P2.5 to P97.5 spread of the measured data.

Overlaid on this measured scatter are the modeled tilt curves computed using (11): solid lines for a 0.07° tilt (bubble within the circle) and dashed lines for a 0.5° tilt. The 0.5° tilt represents a sensor that is clearly not level, with the bubble visibly displaced to one side of the vial, well outside the manufacturer's installation specifications. The center column shows North/South tilts and the right column shows East/West tilts. A "north-facing tilt" means the sensor surface is tilted toward the north (south side raised), so the bubble shifts toward the high side. The name convention applies for the other tilt orientations.

For the North/South tilt (center column), the model predicts the largest percent differences at solar noon when the sun is due south. A north-tilted sensor receives less direct beam at noon (negative percent diff), while a south-tilted sensor receives more (positive percent diff). In the early morning and late afternoon, when the sun is due east or west, cos(A - φ) = cos(90°) = 0 for a North or South tilt, so AOI ≈ Z and the percent difference approaches zero.

For the East/West tilt (right column), the model predicts the largest percent differences in the morning and afternoon when the sun is low in the east or west. An east-tilted sensor receives more direct beam in the morning (positive percent diff) and less in the afternoon (negative percent diff), while a west-tilted sensor shows the opposite pattern. At solar noon, when the sun is due south, cos(AOI) ≈ cos(Z) for an East or West tilt because the azimuth term cos(A - φ) = cos(90°) = 0. The percent difference therefore approaches zero.

The key result is visible in Fig. 4: for all four tilt orientations, the 0.07° tilt lines (representing a realistic leveling error with the bubble within the circle) are entirely contained within the gray noise band for all three sensors. The predicted tilt effect is indistinguishable from the natural day-to-day variability in responsivity. Only when the tilt reaches 0.5° do the modeled curves begin to emerge from the measurement noise. At this level, the bubble would be clearly displaced outside the reference circle, a condition any operator would recognize and correct. This confirms that standard bubble-level alignment provides sufficient precision for pyranometer calibration, and that the day-to-day variation in responsivity is driven by atmospheric conditions rather than residual leveling errors. These results are summarized in Table 2. The tilt effect at the bubble-in-circle level is approximately 10x smaller than the natural measurement variability.

Table 2. Modeled tilt effect compared to measured day-to-day variability.

Tilt Angle	Max %error (solar noon)	Day-to-day P95 spread
0.07° (bubble in circle)	~0.04%	~0.3-0.5%
0.5° (bubble outside)	~0.3%	~0.3-0.5%

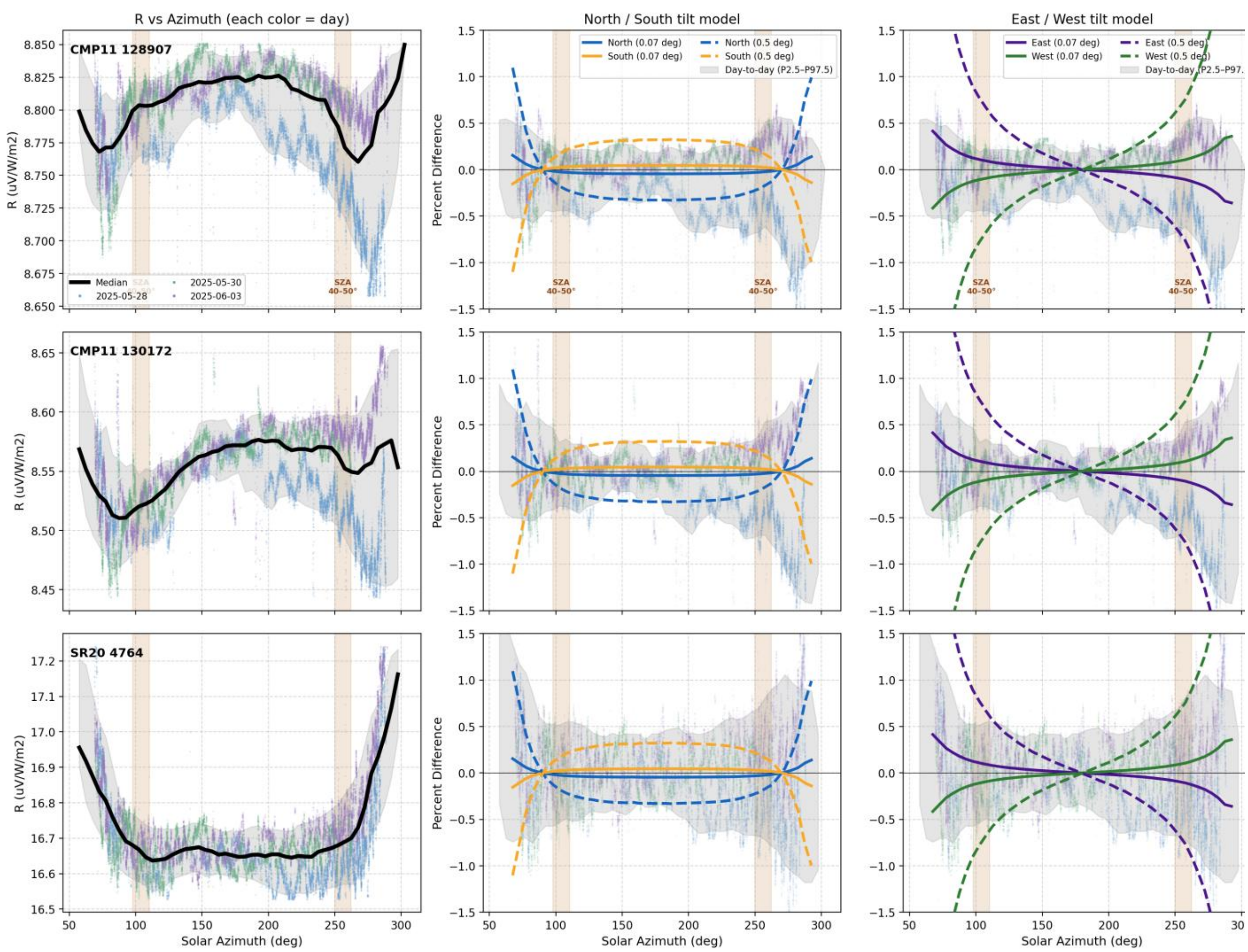

Fig 4. Main result: 3x3 grid showing three sensors (rows) across three views (columns). Left: responsivity versus solar azimuth for three calibration days, with median (black line) and P2.5 to P97.5 band (gray). Center: percent difference from median with North/South tilt model overlaid. Right: percent difference with East/West tilt model overlaid. Solid lines = 0.07° tilt, dashed lines = 0.5° tilt.

It is worth noting that the tilt effect described by (11) is purely geometric. It depends only on the dot product of the sun vector and the surface normal, with no sensor-specific properties (spectral response, temperature coefficient) involved. The magnitude of the effect depends on both the solar zenith angle and the alignment between the tilt direction and the sun azimuth. For North/South tilts, the maximum effect occurs at solar noon when Z is small, limiting the magnitude. For East/West tilts, the maximum occurs at sunrise and sunset when Z is large, which would amplify the effect, but these are also the times when dome directional response errors and atmospheric variability are largest, making any tilt signal difficult to isolate.

An experimental measurement of the tilt effect was also attempted by physically tilting the sensors and calibrating them in the tilted configuration. However, the day-to-day variation in responsivity was comparable to or larger than the expected tilt signal, making the experimental results difficult to interpret. The geometric model provides a clearer path to quantifying the effect.

V. Conclusion

This study established a quantitative relationship between bubble level position and sensor tilt angle for three pyranometer types. For the CMP11 and SR20, the bubble halfway out of the painted reference circle corresponds to a tilt of approximately 0.07°, while the bubble at the circle edge corresponds to 0.13°.

A geometric model was developed to predict the calibration bias from these small tilts. For a 0.07° tilt, the predicted percent difference in responsivity is approximately 0.04%, which is well below the 0.3 to 0.5% day-to-day variability observed in horizontal calibration data. The observed variations in responsivity from one day to the next are not caused by leveling issues, but rather by changes in atmospheric conditions such as water vapor, aerosol loading, and temperature.

As long as the bubble level remains within the painted reference circle, the pyranometer calibration responsivity is not meaningfully affected by residual leveling errors. Standard bubble-level alignment is sufficient for component summation calibrations, and no additional tilt correction is needed. That said, operators should still make reasonable efforts to center the bubble. Other factors such as reference sensor calibration accuracy, optical alignment of the pyrheliometer, sensor cleanliness, and selection of stable clear-sky days have a greater impact on calibration quality and deserve continued attention.

Acknowledgements

The University of Oregon Solar Radiation Monitoring Laboratory (SRML) is sponsored by the National Renewable Energy Laboratory, Bonneville Power Administration, the Energy Trust of Oregon, and Sandia National Laboratories.

The information, data, or work presented herein was funded in part by the Bonneville Power Administration under Award Number 96686. The views and opinions of authors expressed herein do not necessarily state or reflect those of the United States Government or any agency thereof.

References

[1] I. Reda, T. Stoffel, D. Myers, "A method to calibrate a solar pyranometer for measuring reference diffuse irradiance," Solar Energy, vol. 74, no. 2, pp. 103-112, 2003.

[2] ASTM E824-05, "Standard test method for transfer of calibration from reference to field radiometers."

[3] IEA PVPS Task 16, "Best Practices Handbook for the Collection and Use of Solar Resource Data for Solar Energy Applications: Third Edition," Report IEA-PVPS T16-02:2021, April 2021.

[4] L. Menyhart, A. Anda, Z. Nagy, "A new method for checking the leveling of pyranometers," Solar Energy, vol. 120, pp. 25-34, 2015.

[5] L. Vuilleumier, M. Hauser, C. Félix, F. Vignola, P. Blanc, A. Kazantzidis, and B. Calpini, "Accuracy of ground surface broadband shortwave radiation monitoring," J. Geophys. Res. Atmos., vol. 119, pp. 13,838–13,860, 2014.

[6] E. Dutton, C. Long, M. Wild, A. Ohmura, J. Groebner, and A. Roesch, "Long-term in-situ surface flux data products," GEWEX Radiative Flux Assessment (RFA), Vol. 1, WCRP Rep. 19/2012, pp. 135–158, 2012.

[7] F. Vignola, J. Michalsky, and T. Stoffel, *Solar and Infrared Radiation Measurements*, 2nd ed., CRC Press, 2020.